

Three-stage nucleation and growth of Ge self-assembled quantum dots grown on partially relaxed SiGe buffer layers

H. J. Kim,* Z. M. Zhao, and Y. H. Xie

Department of Materials Science and Engineering, University of California Los Angeles, Box 951595, Los Angeles, California 90095-1595, USA

(Received 21 April 2003; revised manuscript received 4 August 2003; published 19 November 2003)

Three-stage nucleation and growth of Ge self-assembled quantum dots (SAQDs) on a relaxed SiGe buffer layer has been studied. Plastic relaxation of the SiGe buffer layer is associated with a network of buried 60° dislocations leading to an undulating strain field. As a result, the surface possesses three different types of sites for the nucleation and growth of Ge SAQDs: over the intersection of two perpendicular buried dislocations, over a single dislocation line, and in the region beyond one diffusion length away from any dislocation. Ge SAQDs are observed to nucleate exclusively over the dislocation intersections first, followed by over single dislocation lines, and finally in the region far away from dislocations. By increasing the Ge coverage at a slow rate, the prenucleation stage at the various sites is observed. It appears that the varying strain field has a significant effect on both the diffusion of Ge adatoms before SAQD nucleation, as well as the shape evolution of the SAQDs after they form. Moreover, two distinctly different self-assembly mechanisms are observed at different sites. There exist denuded zones free of Ge SAQDs adjacent to dislocation lines. The width of the denuded zone can be used to make direct determination of the Ge adatom diffusion lengths. The partially relaxed substrate provides a useful experimental vehicle for the in-depth understanding of the formation mechanism of SAQDs grown epitaxially in the Stranski-Krastanov growth mode.

DOI: 10.1103/PhysRevB.68.205312

PACS number(s): 68.55.Ac, 68.65.Hb

I. INTRODUCTION

Ordering of three-dimensional self-assembled quantum dots (SAQDs) has been an important subject for device applications such as quantum dot lasers.^{1,2} Among the various approaches,^{3–8} the one with a buried stressor appears to be very promising for being the one that does not require fine lithographic techniques that are usually associated with throughput limitations. It has been well known that Ge SAQDs grown on a relaxed SiGe buffer layer preferentially nucleate along buried dislocations.^{6,9} In cubic semiconductors such as Si, Ge, and most III-V compound semiconductors, dislocations of mixed edge-screw type¹⁰ with the angle between Burgers vector and the dislocation line being 60° move fast through glide mechanism. As a result, they dominate the dislocation population. For the typical combination of a (001) substrate and a lattice mismatched epitaxial thin film, 60° dislocation lines lie at the film-substrate interface, run along $\langle 110 \rangle$ directions and form rectangular arrays.

In this study, partially relaxed SiGe buffer layers with buried 60° dislocation arrays are used as the stressor. In contrast to previous studies that aimed at obtaining regular SAQD placement,⁶ dislocation spacing in the current study is carefully controlled to be significantly larger (instead of smaller) than the surface diffusion length of Ge adatoms. Typical duration of the high temperature processes when the adatom motion is rapid is around 120 sec in our experiments. The diffusion length is on the order of $0.5 \mu\text{m}$. For an average dislocation spacing of $\sim 7 \mu\text{m}$, three types of surface sites can be distinguished from one another and monitored with ease. The three types of sites include those over the dislocation intersections (site A), those over single disloca-

tion lines (site B), and those far away from dislocations (site C).

From the standpoint of adatom density, Stranski-Krastanov (SK) growth mode itself is an interesting contrast to the growths of Si on Si that proceeds in the Frank-van der Merwe (FV) mode. The latter has been studied in detail by Mo *et al.*¹¹ and has been shown to grow via either step propagation or two-dimensional (2D) island nucleation and coalescence. As a result, the adatom density reaches a steady state value for a given incident molecular flux and remains at that value throughout the rest of the growth process. SK growths such as Ge on Si or InAs on GaAs, on the other hand, go through FV mode during the first couple of monolayers coverage, i.e., during the formation of the wetting-layer. At the completion of the wetting-layer formation, surface steps cease functioning as sinks for adatoms and 2D island nucleation and growth are prohibited energetically. As a result, the adatom density starts to increase linearly with time until it reaches the supersaturation value for the nucleation of SAQDs. The three types of sites on the surface of a partially relaxed buffer layer have the difference in their in-plane lattice constants with the value at A sites being the closest to that of unstrained Ge. Intuitively, such differences can translate into either a difference in the diffusion coefficient of the adatoms, in the wetting-layer thickness, in the critical size of pyramid-to-dome transition,¹² or all of the above. This paper attempts to provide answers to some of these questions.

Through fine control of the Ge coverage to a fraction of an angstrom, prenucleation ridges over single dislocation lines are observed immediately before the formation of Ge islands, i.e., SAQDs. Ge SAQDs formed subsequently have the characteristic pyramid shape. With increased Ge cover-

age, these pyramids undergo a transition to domes, i.e., islands with a multitude of higher angle facets.¹³ The critical island size at which the pyramid-to-dome transition takes place is different between the SAQDs located over the three different types of sites. Under the assumption that the transition represents a switch over in the minimum free energy shape as proposed by Ross *et al.*,¹⁴ the difference in the critical island size can be taken as an indicator of the difference in misfit strain energy among the three types of sites.

There are well-defined denuded zones on both sides of the buried dislocations that are free of Ge SAQDs. The nucleation of SAQDs at C sites occurs abruptly in terms of Ge coverage. The nucleation process lasts for a duration of approximately 20 sec depending on the Ge flux. A growth interruption of comparable length in time resulted in a lower SAQD density, indicating the importance of the role of surface diffusion. In the region between the initially nucleated dots, the Ge adatom density decreases as a result of surface diffusion in cases with low or zero incident Ge flux. For higher incident Ge flux and the diffusion flux, Ge adatom density in the region between dots may increase with time, resulting in the nucleation of more islands. In the meantime, the average spacing between islands decreases with increasing island density, causing a decrease in the ratio between the incident Ge flux and the surface diffusion flux, and the eventual vanishing of the supersaturation. Nucleation stops as a result.

A further deposition of Ge is associated with an increase in the average SAQD volume and a nearly constant SAQD density. Ostwald ripening is then observed first among SAQDs at site B, presumably due to the close spacing between dots. The surface diffusion under the influence of an undulating chemical potential on a strained surface was examined by Freund.¹⁵ Mattsson *et al.* simulated the nucleation of three-dimensional islands on a strained surface.¹⁶ The experimental observations presented in this paper will provide a more solid basis for theoretical calculations and simulations, thereby furthering the understanding of this scientifically challenging and technologically important formation mechanism of semiconductor SAQDs.

II. EXPERIMENTAL DETAILS

Samples used in this study were grown by a Riber EVA-32 molecular beam epitaxy system equipped with two electron beam evaporation sources of Si and Ge, respectively. All samples consist identical relaxed SiGe buffer structures that provide the undulating strain field. The partially relaxed buffer layers were prepared by the following sequence. First, p-type Si(001) substrates with 10 Ω -cm resistivity were sent through a wet chemical cleaning process known as modified Piranha.¹⁷ The chemical oxide layer was subsequently removed in-situ at a substrate temperature of 800 °C in a low Si flux of 0.2 $\text{\AA}/\text{s}$. An 800 \AA thick $\text{Si}_{0.9}\text{Ge}_{0.1}$ buffer layer and a 100 \AA thick Si cap layer were grown at 550 and 600 °C, respectively. The buffer layer was almost completely strained as grown. Then the samples underwent a post-growth anneal at 700 °C for 30 min that led to the partial strain relaxation of the $\text{Si}_{0.9}\text{Ge}_{0.1}$ buffer layer via dislo-

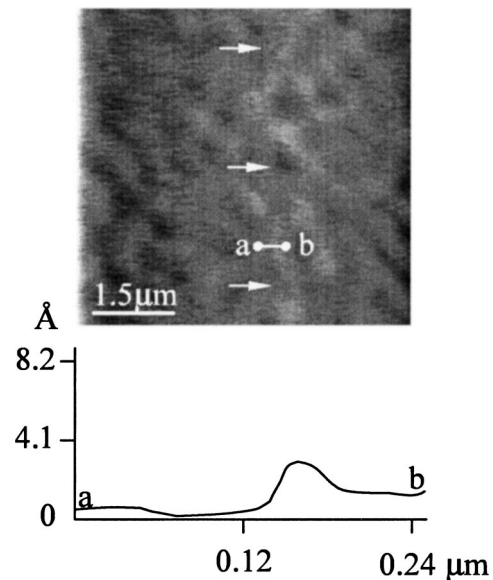


FIG. 1. Two-dimensional AFM topographic image of the sample before Ge growth. Arrows indicate the ridge on the top surface resulting from buried single dislocation. The line scan of a-b illustrates that the ridge height across buried single dislocation is $2.9 \pm 0.7 \text{ \AA}$.

cation. The function of the Si cap layer under tensile strain is to preserve a flat surface.¹⁸ The resulting samples consist of an undulating strain field with a relatively flat top surface of Si atoms (rms on the order of a few angstroms). The quality of the resulting surface was examined using reflection high-energy electron diffraction. Streaky 2×1 patterns were observed for all samples throughout the growth and annealing processes.

Ge SAQDs growths were carried out at 700 °C with Ge coverage ranging from 3.0 to 12.0 \AA . All samples employed the slow growth rate of 0.05 $\text{\AA}/\text{s}$. After Ge growths, the samples were quenched to room temperature. Ge SAQDs grown at the various Ge coverage were characterized with a Park Scientific atomic force microscopy (AFM) operating in contact mode. Surface topography, in particular the ridges over single dislocation lines as well as the shape and dimension changes of Ge dots at three different sites, were carefully characterized for samples of various Ge coverage. The fidelity of the AFM topography is ensured by the low aspect ratio of the Ge SAQDs [the typical aspect ratio of pyramids grown on bulk Si(001) substrate is around 1:10] relative to the AFM tip radius. The radius of the AFM tip used in the study is $\sim 20 \text{ nm}$. The location of the buried dislocations was revealed by lines of steps such as the one shown in Fig. 1. Arrows indicate the step over a buried single dislocation line. To ensure the exclusive existence of SAQDs at site A in the case of low Ge coverage, scan sizes as large as $60 \times 60 \mu\text{m}^2$ were used.

III. RESULTS

A. Observation of three-stage nucleation

AFM topography of samples with Ge coverage of 4.0, 4.5, 5.0, and 6.0 \AA are shown in Fig. 2 (a)–(d). The first

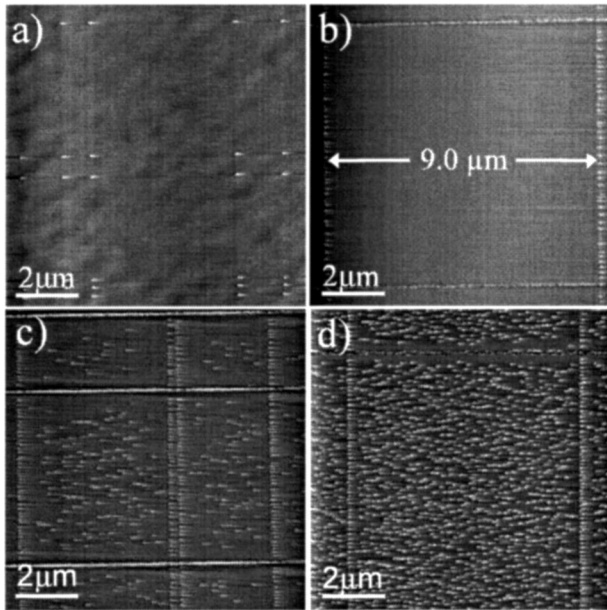


FIG. 2. Two-dimensional AFM topographic images of Ge SAQDs with 4–6 Å coverage on a partially relaxed $\text{Si}_{0.9}\text{Ge}_{0.1}$ buffer layer. (a) 4.0 Å Ge coverage with Ge SAQDs only at site A. (b) 4.5 Å Ge coverage with Ge SAQDs at sites A and B. (c) 5.0 Å Ge coverage with Ge SAQDs at sites A, B, and C. (d) 6.0 Å Ge coverage with Ge SAQDs at sites A, B, and C.

three images clearly illustrate the existence of three types of surface sites and the resulting three-stage nucleation at dislocation intersections [type A, (a)], single dislocation lines [type B, (b)], and in regions far away from dislocations [type C, (c)], respectively. Three-stage nucleation is clearly shown as the Ge coverage increases. At 4.0 Å, Ge SAQDs of pyramidal shape nucleate exclusively at A sites. These pyramids form a rectangular array with perfect registry to the network of buried dislocations. The pyramids show an aspect ratio of around 1:10.8 (± 1) representing slightly lower angle facet than the well-known {105}. It is believed that this low aspect ratio is caused by the kinetically limited growth at the experimental parameters used in this study. An additional 0.5 Å of Ge growth causes the preferential nucleation of Ge SAQDs over dislocation lines (site B). Figure 2(b) shows a large rectangle bordered by dislocations consisting of SAQDs formed at A and B sites. Although the Ge coverage at this point is approximately the wetting-layer thickness [established in the literature to be $\sim 3 \text{ ML} \approx 4.2 \text{ \AA}$ in the case of Ge grown on bulk Si(001) substrate¹⁹], it is important to notice that there is no SAQD in the region between dislocations. The dislocation spacing of $\sim 9 \mu\text{m}$ is much larger than surface diffusion length of Ge adatom reported in literature^{20,21} under similar conditions. The appearance of SAQDs at sites A and B indicates that either the Ge adatom density is higher or the nucleation barrier is lower at these sites.

B. Prenucleation stage

In an effort to differentiate between the two possibilities, the surface topography immediately prior to the nucleation

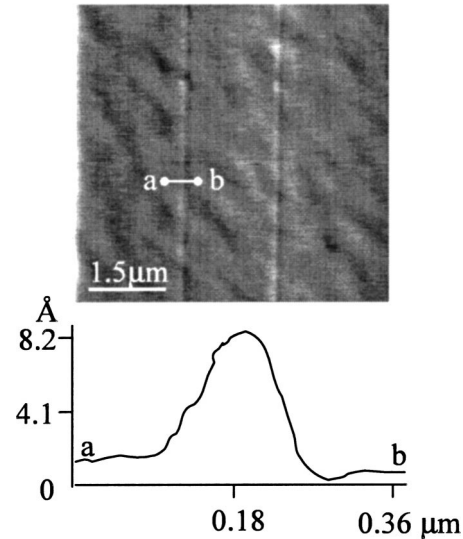


FIG. 3. Two-dimensional AFM topographic image of the sample with 3.0 Å Ge. The line scans of a-b illustrates that the ridge height across a buried single dislocation is $7.5 \pm 1.5 \text{ \AA}$.

of any islands was examined in detail. Evidence of a higher density of Ge adatoms is observed at site B in the form of a ridge (not islands) of very low aspect ratio as shown in Fig. 3. The ridge height in samples with 3.0 Å Ge coverage was determined to be $7.5 \pm 1.5 \text{ \AA}$, a significant increase from the $2.9 \pm 0.7 \text{ \AA}$ value in the sample with no Ge coverage. The original ridge height from samples with no Ge coverage agrees well with the observation by Lutz *et al.*²² who claimed a ridge height of $2.5 \pm 0.3 \text{ \AA}$ for individual buried dislocations. Although there are definite non-planarity at these sites, (001) remains to be the prevailing facets. The average terrace width of $\sim 240 \text{ \AA}$ calculated from the aspect ratio of the ridges is comparable to that on typical Si(001) surfaces. The only difference is the polarity of the “force dipole” at these steps²³ are more aligned. We call these ridges “pile-ups” of Ge in order to differentiate them from SAQDs. The lack of 3D Ge islands at this Ge coverage indicates that the wetting-layer thickness ($> \sim 4.5 \text{ \AA}$) at these sites is much thicker than at site C, presumably due to the much reduced misfit strain at these sites. The above observation favors the higher Ge adatom density possibility over that of a lower nucleation barrier at B sites.

A similar pile-up of Ge is also observed at site A. There, due to the fourfold symmetry, the pile-ups are in pyramidal shape with extremely low ($\sim 1:145$) aspect ratio. Furthermore, the aspect ratio seems to vary continuously with time, instead of staying at a constant value such as in the case of typical Ge pyramids on Si. The fact that no single facet is preferred indicates that such pile-ups of Ge are not SAQDs. In other words, they do not represent energetically stable islands. Instead, they could be explained by the existence of a chemical potential gradient for Ge adatoms toward A and B sites caused by the undulating strain field. Supporting this belief is the fact that such pile-ups are never observed at site C, where there is no directional diffusion of Ge adatoms.

C. Observation of simultaneous SAQDs growth and nucleation

A Ge coverage beyond 4.5 Å causes the adatom density at site C to reach the supersaturation level for 3D island nucle-

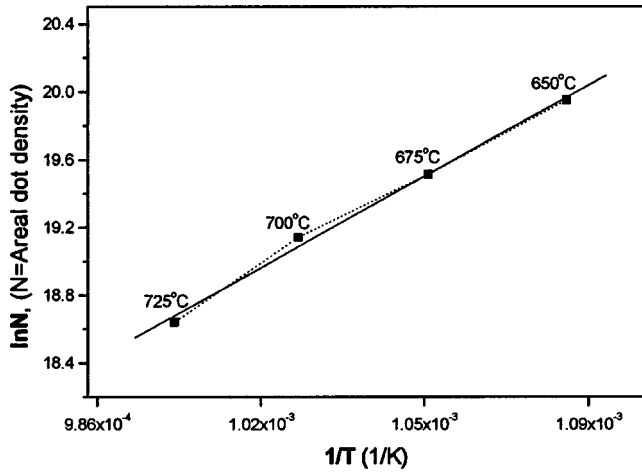


FIG. 4. The measured areal dot density as a function of the growth temperature for Ge SAQDs. The Arrhenius plot shows the activation energy of 0.682 ± 0.04 eV.

ation. At 5.0 \AA Ge coverage, randomly distributed SAQDs with a rather low density ($\sim 6.5 \times 10^8 \text{ cm}^{-2}$) appear at site C [Fig. 2(c)]. Subsequent Ge growth causes the line density at site B to increase to a maximum value of $\sim 9.2 \times 10^4 \text{ cm}^{-1}$. There is a corresponding areal density increase at site C to $\sim 1.7 \times 10^9 \text{ cm}^{-2}$. Interestingly, the maximum SAQD densities at sites B and C are both reached at the Ge coverage of 6.0 \AA . The dot density remains constant upon continued deposition of Ge from 6.0 to 8.0 \AA . In other words, there exists a period during the growth (that corresponds to Ge coverage between 6.0 and 8.0 \AA under the current experimental conditions) when the Ge adatom supersaturation falls below the value necessary for the nucleation of Ge islands. This happens when the incident Ge flux can no longer replenish the loss of Ge adatoms due to surface diffusion in regions between dots. Beyond a 8.0 \AA Ge coverage, coarsening sets in that will be discussed below.

D. Different determining factors for the interdot spacing at different sites

It is worth noting that the spacing between Ge SAQDs at site B is significantly smaller than that at site C. For example, in the sample with 6.0 \AA Ge [Fig. 2(d)], the spacing between adjacent dots of $\sim 0.02 \mu\text{m}$ at site B is about an order of magnitude smaller than the value of $\sim 0.24 \mu\text{m}$ at site C. One possible reason contributing to this difference is the anisotropic nature of strain in the dots at site B. The misfit strain between the dots and the substrate is less in the direction perpendicular to the underlying dislocation lines. The consequence of the close spacing is that there is strong elastic interaction between dots via the substrate. In other words, the dot spacing is likely to be determined by the interaction via the elastic strain field in the near surface region of the substrate. This is in clear contrast with the much larger spacing between dots at site C. At site C, the spacing between dots is determined by the surface diffusion length of Ge adatoms. The spacing varies with the substrate temperature in an Arrhenius fashion as shown in Fig. 4. The activa-

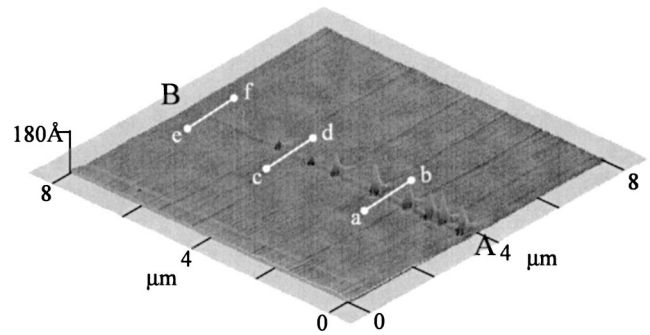


FIG. 5. Three-dimensional AFM topographic images of the sample in which the nucleation of Ge SAQDs proceeds along an underlying dislocation. Ridge heights across a single dislocation of a-b, c-d, and e-f are ~ 7.2 , ~ 4.8 , and $\sim 2.9 \text{ \AA}$, respectively.

tion energy extracted from such Arrhenius behavior is approximately 0.682 ± 0.04 eV, in close agreement with the well established value for surface diffusion of Ge on Si.^{24,25} This observation provides strong evidence that the spacing between dots at site C is determined by surface diffusion of Ge adatoms.

E. Evidence of difference in misfit strain among SAQDs at different sites

Finally, the critical size of pyramid-to-dome transition is used for qualitative comparison of misfit strain in SAQDs at sites A, B, and C. The critical size is characterized by the base diameter of the smallest domes and the largest pyramids. Ross *et al.*¹⁴ suggested that the transition represents the free energy crossover point at which islands with a multitude of larger angle facets become more stable than pyramids. As a result, the critical size should be dependent on, and can be used as an indicator of, the misfit strain in SAQDs. The critical sizes at the three different sites can be measured experimentally at Ge coverage of slightly below 6.0 \AA for which both pyramids and domes coexist. The critical sizes of SAQDs at sites A, B, and C are determined to be 1237 ± 10 , 1041 ± 10 , and $886 \pm 10 \text{ \AA}$, respectively. This observation provides indirect evidence that the misfit strain is the lowest at site A and the highest at site C.

F. Observation of a rare event of SAQDs forming after a single propagating dislocation

During our study, we came across a rare event that is, we believe, the result of dot formation along a buried dislocation half loop that is expanding. In Fig. 5 the nucleation of Ge SAQDs proceeds from point A to point B along buried single dislocation. The dot size becomes smaller and the dots spacing becomes larger as we move from the center towards the end of the dislocation half loop. This trend is symmetric towards the other end of the dislocation. Three line scans reveal that ridge heights of a-b, c-d, and e-f are 7.2 , 4.8 , and 2.9 \AA , respectively. This trend is a direct consequence that the accumulation of Ge adatoms by surface diffusion happens at a finite rate. The time it takes is comparable to the

time it takes for the dislocation to expand by several μm . As a result, the time period during which directional surface diffusion happens is noticeably shorter near the end of the buried dislocation half loop comparing to that near the center. The ridge height of e-f is comparable to the one in samples without Ge growth corresponding to Fig. 1, whereas that of a-b is practically the value measured across any buried dislocation line in Figs. 2(a) or 2(b). The total length of this propagating buried dislocation is found to be $\sim 24 \mu\text{m}$ by following the ridge. Apparently, the dislocation half loop was introduced near the beginning of the Ge growth that took place at 700°C . Such a substrate temperature is sufficient to allow a dislocation half loop to grow at a rate that is on the order of a few μm per minute.²⁶ The formation of the dots along the line is practically trailing the expanding dislocation, allowing us to observe the unfolding of such a dynamic process.

IV. DISCUSSION

The experimental observations presented in this study show the kind of information that can be extracted by using a partially relaxed buffer layer. It is an excellent experimental vehicle for the study of the various stages of nucleation and growth of SAQD formation in the SK mode. There is a complex interplay of the directional surface diffusion of Ge adatoms with the different SAQD nucleation barriers at the various surface sites. The experimental results provide insight into the formation process of Ge SAQDs on Si. At the same time, these results also raise more unknowns.

Following the evolution of the Ge adatom density near the three different types of sites on the surface, we can “trace” the formation of Ge SAQDs on Si(001). At the beginning of the growth, the Ge adatom density increases all across the sample surface. Together with this increase, directional diffusion takes place, presumably as a result of the difference in the Ge adatom diffusivity near the three types of surface sites. Ge adatoms dwell longer at sites A and B because the lattice constants there are closer to that of unstrained Ge. Consequently, there is a net flux of Ge adatoms from the surrounding region towards sites A and B, and the Ge density near these sites increases as a result. The wetting-layer thickness at these sites is apparently much larger than on bulk Si surfaces ($\sim 4.2 \text{ \AA}$, as is well established in the literature). There is no SAQD nucleation at site B for Ge layer thickness values of $< \sim 6.0 \text{ \AA}$. Such a large wetting-layer thickness can again be explained using the much lowered misfit strain between the SAQDs and the substrate at sites A and B compared to that at site C. Intuitively, a zero misfit strain should lead to a wetting-layer thickness approaching infinity.

Directional diffusion leads to a partial depletion of Ge adatoms near sites A and B that is later manifested as a “denuded zone” free of SAQDs. The extent of the directional diffusion is approximately the diffusion length during the experimental process, and is on the order of μm . As a result, the Ge adatom density in regions far away from site A and B is largely unaffected. It is expected to stay constant first until the completion of the wetting layer. At that point, step edges stop functioning as sinks for adatoms and 2D

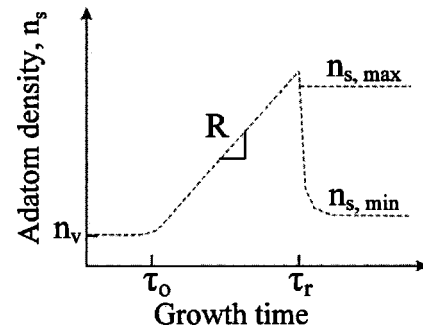


FIG. 6. Schematic drawing of the adatom density (n_s) as a function of growth time (t) at a growth rate of R . The wetting layer is completed at τ_0 and 3D SAQD nucleation occurs at τ_r . n_v is equilibrium adatom density.

nucleation becomes energetically unfavorable, the Ge adatom density starts to increase within deposition time in a linear fashion. Figure 6 depicts the expected evolution of the Ge adatom density with time.

Upon an increase of the Ge coverage, SAQD nucleation begins first at site A, and then at site B. All dots begin with a pyramidal shape that is followed by an abrupt transition to the well-known dome shape.¹³ The reason that SAQDs form at sites A and B is interpreted as a result of the abundant supply of Ge adatoms due to the strain induced chemical potential gradient. Although no appropriate experiments have yet been done, it is expected that the amount of time during which the substrate temperature is sufficiently high is the determining factor for the preferential nucleation of SAQDs at sites A and B. The degree of supersaturation at these sites increase with the duration.

A further increase of the Ge coverage eventually leads to the nucleation of SAQDs at site C. This occurs when the Ge supersaturation reaches the critical value for SAQD nucleation. The combined knowledge of the Ge flux and the deposition time allows a rough estimate of the critical value of the Ge supersaturation necessary for the nucleation of SAQDs. The only uncertainty in such an estimate is the precise wetting-layer thickness that cannot be determined by the absence of SAQDs, but only by monitoring the adatom density in real time. The majority of the wetting-layer information quoted in the literature uses the former definition and is therefore strictly speaking inaccurate.

Immediately after the onset of SAQD nucleation at site C, directional diffusion takes place across the entire sample surface. At this point, all existing SAQDs function as sinks for Ge adatoms. Figure 7 shows a schematic drawing of the Ge adatom density near SAQDs at site C. Directional diffusion contributes to the decrease of the Ge adatom density between dots. The rate of decrease is inversely proportional to the interdot spacing. If the incoming Ge flux is higher than the directional diffusion rate, the Ge adatom density between dots will increase. Such an increase in the adatom density leads to a continued nucleation of SAQDs and consequently to a decrease in the interdot spacing. The result is an increase in the rate of directional diffusion. This process continues until a quasisteady state is reached in which the incoming Ge flux is equal to the directional diffusion rate, and SAQD nucleation stops as a result. During this process, experimen-

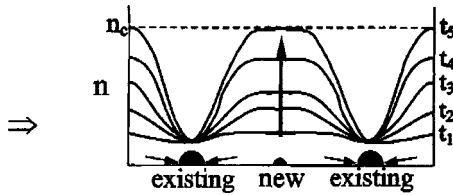


FIG. 7. Schematic drawing of the Ge adatom density between two existing Ge SAQDs at site C. When the distance between the two dots is larger than the equilibrium interdot spacing, another nucleation occurs at the position Ge super saturation reaches the critical value (n_c) with the increase of time (t_1 to t_5).

tal observations show a continued nucleation of SAQDs that corresponds to a Ge coverage from 4.5 to 6.0 Å in our experiments. Eventually, the spacing between dots becomes small enough so that the directional diffusion flux overtakes the incoming Ge flux and the Ge adatom density drops below the critical supersaturation value (n_c). The SAQD nucleation process comes to a halt. This point happens at a 6.0 Å Ge coverage in our experiments.

Ostwald ripening is going on throughout this process ever since the formation of SAQDs. The ripening process manifests itself as a widening of the SAQD size distribution. The larger dots grow larger at the expense of smaller ones. In the case of a higher Ge supersaturation value, ripening takes place simultaneously with the growth in size for both small and large dots. As the Ge adatom density eventually decreases to below the equilibrium value for smaller dots, but still above that for larger dots, smaller dots start to shrink in size and the effect of the ripening process becomes more obvious. Figure 8 shows the evolution of the dot size distribution as a function of the growth time (Ge coverage). It is obvious that after an 8.0 Å Ge coverage, the effect of ripening becomes increasingly visible. Coarsening at site B becomes apparent at a much earlier stage because of the close spacing between dots.

The observation that SAQD nucleation trails an expanding dislocation half loop provided valuable insight into the

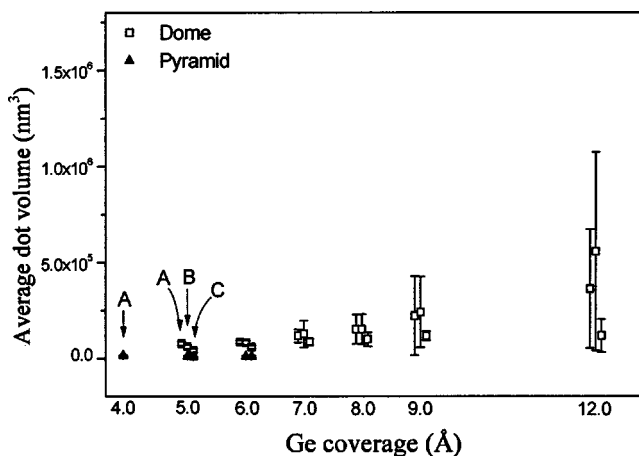


FIG. 8. The evolution of the average dot volumes at three different surface sites (A, B, and C) as a function of the growth time. A bimodal distribution consisting of pyramids and domes remains up to 6.0 Å Ge coverage.

formation of SAQDs over dislocations. It showed us that the average spacing between dots at site B is not always that small. It becomes smaller with time and eventually reaches a value of $\sim 0.02 \mu\text{m}$ as limited by the substrate strain field. Our observation points to the natural next step in the experiment, i.e., using *in situ* transmission electron microscopy to follow the expanding dislocation loop and the subsequent formation of SAQDs. Such a study will provide direct evidence of the directional diffusion rate of Ge adatoms that begins after the dislocation expands beyond a given point and results in the formation of SAQDs a short while later.

Continued Ge deposition eventually result in the average SAQD size to increase beyond the point when dislocation formation becomes energetically favorable. The dominant dot shape evolves from domes to superdomes.²⁷ This latest regime is associated with dislocated SAQDs that are not suitable for most electronic and optoelectronic applications. Consequently, it will not be discussed further.

For a partially relaxed SiGe buffer layer with an average dislocation spacing smaller than Ge diffusion length, only sites A and B are operational. For even higher dislocation density, SAQDs could be grown under the regime in which only site A is active. That is the regime used to demonstrate rectangular arrays of SAQDs by more than one groups.^{6,28}

While insightful information has resulted from our experiments, several questions remain. First of all, the quantitative relation between misfit strain and the chemical potential for Ge surface diffusion is not known. Unlike metal systems such as Ag/Ag(001) for which studies have been conducted, surface reconstruction in semiconductors makes the situation more complex. The observed preferential nucleation and growth over dislocations is likely to come from the combined effect of chemical potential gradient for individual quantum dots and the varying energy barrier for the surface diffusion of Ge adatoms. More carefully planned experiments combined with theoretical studies are necessary to further our understanding on this subject. Moreover, a proper way to define the wetting-layer thickness over a ridge at site B warrants further debate. Finally, the exact reason for the one order of magnitude smaller spacing between SAQDs over a dislocation comparing to that at site C is not clear. Further experiments should be constructed to clarify these points.

V. CONCLUSION

In summary, the use of partially relaxed SiGe buffer layers with an average dislocation spacing larger than the Ge surface diffusion length proves to be a powerful approach for understanding the nucleation and growth mechanism of Ge SAQDs on a Si substrate. Clear evidence of descending chemical potential fields around buried dislocations was observed. The wetting-layer thickness over dislocations is significantly larger than other areas. An approach is established that allows us to quantitatively measure the critical supersaturation value for Ge on Si for the nucleation of SAQDs. A rare event of SAQD formation following an expanding dislocation half loop provided further insight into the formation of SAQDs over dislocations. An Ostwald ripening has been

clearly observed that occurs at different rates over the various surface sites. Such experimental observations provide a wealth of information for furthering our understanding of the formation mechanism of Ge SAQDs on Si.

ACKNOWLEDGMENTS

The work was partly supported by Army Research Office (ARO) (Grant No. DAAD19-01-1-0532).

*Email address: kimhj@ucla.edu

- ¹N. Kirstaedter, N. N. Ledentsov, M. Grundmann, D. Bimberg, V. M. Ustinov, S. S. Ruvimov, M. V. Maximov, P. S. Kop'ev, Zh. I. Alferov, U. Richter, P. Werner, U. Gösele, and J. Heydenreich, *Electron. Lett.* **30**, 1416 (1994).
- ²Zh. I. Alferov, *Phys. Scr.* **68**, 32 (1996).
- ³S. Y. Chou, P. R. Krauss, and L. Kong, *J. Appl. Phys.* **79**, 6101 (1996).
- ⁴U. Drodofsky, J. Stuhler, T. Schulze, M. Drewsen, B. Brezger, T. Pfau, and J. Mlynek, *Appl. Phys. B* **65**, 755 (1997).
- ⁵C. Teichert, M. G. Lagally, L. J. Peticolas, J. C. Bean, and J. Tersoff, *Phys. Rev. B* **53**, 16334 (1996).
- ⁶Y. H. Xie, S. B. Samavedam, M. Bulsara, T. A. Langdo, and E. A. Fitzgerald, *Appl. Phys. Lett.* **71**, 3567 (1997).
- ⁷A. E. Romanov, P. M. Petroff, and J. S. Speck, *Appl. Phys. Lett.* **74**, 2280 (1999).
- ⁸F. Leroy, J. Eymery, P. Gentile, and F. Fournel, *Appl. Phys. Lett.* **80**, 3078 (2002).
- ⁹H. J. Kim, J. Y. Chang, and Y. H. Xie, *J. Cryst. Growth* **247**, 251 (2003).
- ¹⁰E. A. Fitzgerald, *Mater. Sci. Rep.* **7**, 87 (1991).
- ¹¹Y.-W. Mo, J. Kleiner, M. B. Webb, and M. G. Lagally, *Surf. Sci.* **268**, 275 (1992).
- ¹²H. J. Kim and Y. H. Xie, *Appl. Phys. Lett.* **79**, 263 (2001).
- ¹³R. S. Williams, G. Medeiros-Ribeiro, T. I. Kamins, and D. A. A. Ohlberg, *J. Phys. Chem. B* **102**, 9605 (1998).
- ¹⁴F. M. Ross, J. Tersoff, and R. M. Tromp, *Phys. Rev. Lett.* **80**, 984 (1998).
- ¹⁵L. B. Freund, *Int. J. Solids Struct.* **32**, 911 (1995).
- ¹⁶T. R. Mattsson and H. Metiu, *Appl. Phys. Lett.* **75**, 926 (1999).
- ¹⁷Three times repeating of [(1:10=HF:H₂O)→(H₂O rinse)→(5:3=H₂SO₄:H₂O₂)→(H₂O rinse) for one minute at each step].
- ¹⁸Y. H. Xie, G. H. Gilmer, C. Roland, P. J. Silverman, S. K. Buratto, J. Y. Cheng, E. A. Fitzgerald, A. R. Kortan, S. Schuppler, M. A. Marcus, and P. H. Citrin, *Phys. Rev. Lett.* **73**, 3006 (1994).
- ¹⁹Y.-W. Mo, D. E. Savage, B. S. Swartzentruber, and M. G. Lagally, *Phys. Rev. Lett.* **65**, 1020 (1990).
- ²⁰X. Deng, J. D. Weil, and M. Krishnamurthy, *Phys. Rev. Lett.* **80**, 4721 (1998).
- ²¹T. Schwarz-Selinger, Y. L. Foo, David G. Cahill, and J. E. Greene, *Phys. Rev. B* **65**, 125317 (2002).
- ²²M. A. Lutz, R. M. Feenstra, F. K. LeGoues, P. M. Mooney, and J. O. Chu, *Appl. Phys. Lett.* **66**, 724 (1995).
- ²³O. L. Alerhand and E. J. Mele, *Phys. Rev. B* **35**, 5533 (1987).
- ²⁴D. Srivastava and B. J. Garrison, *Phys. Rev. B* **46**, 1472 (1992).
- ²⁵C. Roland and G. H. Gilmer, *Phys. Rev. B* **47**, 16 286 (1993).
- ²⁶R. Hull, J. C. Bean, D. J. Werder, and R. E. Leibenguth, *Appl. Phys. Lett.* **52**, 1605 (1988).
- ²⁷R. S. Williams, G. Medeiros-Ribeiro, T. I. Kamins, and D. A. A. Ohlberg, *Acc. Chem. Res.* **32**, 425 (1999).
- ²⁸S. Yu. Shiryayev, F. Jensen, J. L. Hansen, J. W. Petersen, and A. N. Larsen, *Phys. Rev. Lett.* **78**, 503 (1997).